Appearance of the universal value e2/h of the zero-bias conductance in a Weyl semimetal-superconductor junction

Rapid Communications

Appearance of the universal value e^2/h of the zero-bias conductance in a Weyl semimetal-superconductor junction

Song-Bo Zhang,[1] Fabrizio Dolcini,[2] Daniel Breunig,[1] and Björn Trauzettel[1]
[1]*Institute for Theoretical Physics and Astrophysics, University of Würzburg, D-97074 Würzburg, Germany*
[2]*Dipartimento di Scienza Applicata e Tecnologia del Politecnico di Torino, I-10129 Torino, Italy*

(Received 22 November 2017; published 25 January 2018)

We study the differential conductance of a time-reversal symmetric Weyl semimetal-superconductor junction with an s-wave superconducting state. We find that there exists an extended regime where the zero-bias differential conductance acquires the universal value of e^2/h per channel, independent of the pairing and chemical potentials on each side of the junction, due to a perfect cancellation of Andreev and normal reflection contributions. This universal conductance can be attributed to the interplay of the unique spin/orbital-momentum locking and s-wave pairing that couples Weyl nodes of the same chirality. We expect that the universal conductance can serve as a robust and distinct signature for time-reversal symmetric Weyl fermions and be observed in the recently discovered time-reversal symmetric Weyl semimetals.

DOI: 10.1103/PhysRevB.97.041116

Introduction. A Weyl semimetal (WSM) is a three-dimensional (3D) topological phase of matter in which the conduction and valence bands touch linearly at discrete points, called Weyl nodes, in the Brillouin zone near the Fermi energy [1–4]. According to the fermion doubling, such Weyl nodes appear in pairs with opposite chirality [5], linked to monopoles and antimonopoles of the field of Berry curvature in momentum space. To ensure nonzero Berry curvature, a WSM must violate either inversion or time-reversal symmetry. This nontrivial momentum-space topology of WSMs gives rise to a variety of intriguing physical phenomena, such as surface Fermi arcs [1], the chiral anomaly [6–9], and associated anomalous transport properties [10–25]. The actual discoveries of WSMs in a growing number of materials [26–42] have spurred interest in investigating the interplay of such topological phase with other electronic phases and orders.

Recently, the possibilities of superconducting states, doping or proximity induced, in WSMs have been discussed [43–56]. Most of the theoretical works investigating hybrid structures based on WSMs focus on the time-reversal broken case [57–63]. However, so far almost all experimentally demonstrated WSMs break inversion symmetry but preserve time-reversal symmetry [30–35]. Importantly, while in a time-reversal broken Weyl superconductor the s-wave pairing couples electrons of opposite chirality, in the time-reversal symmetric case it instead couples electrons of the same chirality [43] so that distinct transport properties in semimetal-superconductor (N-S) junctions could be expected.

In this Rapid Communication, we study a 3D time-reversal symmetric N-S junction constructed by a normal WSM and an s-wave superconducting WSM. Near the Weyl nodes, the intraorbital pairing dominates the superconducting state. Denoting by μ_N and μ_S the chemical potentials of the WSM and the superconductor, respectively, and by Δ_s the superconducting pairing potential, we find that, in the regime $|\mu_N| \ll (|\Delta_s|^2+\mu_S^2)^{1/2}$, the contributions of Andreev and normal reflections perfectly cancel at vanishing excitation energy. In this regime, the zero-bias differential conductance, thus, takes the universal value e^2/h per channel independent of μ_N, μ_S, and Δ_s. We attribute this universal conductance to the interplay of the unique spin/orbital-momentum locking and s-wave pairing in the Weyl junction. We also discuss its robustness and expect that it can serve as a distinct signature for time-reversal symmetric Weyl fermions in clean systems. We are confident that the universal conductance can be observed in the recently discovered time-reversal symmetric WSMs [38–40].

Model Hamiltonian. We start with a low-energy model for a time-reversal symmetric WSM [64]: $\mathcal{H}_{\rm w}=\sum_{\mathbf{k}}\psi^\dagger_{\mathbf{k}}H(\mathbf{k})\psi_{\mathbf{k}}$ and

$$H(\mathbf{k}) = k_x s_x\sigma_z + k_y s_y\sigma_0 + \left(\kappa_0^2-|\mathbf{k}|^2\right)s_z\sigma_0 + \beta s_y\sigma_y - \alpha k_y s_x\sigma_y, \quad (1)$$

where $\mathbf{k}=(k_x,k_y,k_z)$ is the wave vector and the four-component spinor $\psi_{\mathbf{k}}=(c_{A,\uparrow,\mathbf{k}},c_{A,\downarrow,\mathbf{k}},c_{B,\uparrow,\mathbf{k}},c_{B,\downarrow,\mathbf{k}})^T$ is written in terms of annihilation operators $c_{s,\sigma,\mathbf{k}}$ with spin indices $\sigma=\uparrow,\downarrow$ and orbital indices $s=A,B$. Here, σ_i $(i=0,x,y,z)$ are the 2×2 identity and Pauli matrices for the spin-1/2 space and s_i $(i=0,x,y,z)$ for the orbital space. κ_0, α, and β are real model parameters. The model (1) breaks inversion symmetry, i.e., $s_zH(\mathbf{k})s_z\neq H(-\mathbf{k})$ by the β term but preserves time-reversal symmetry as shown by $\sigma_yH^*(\mathbf{k})\sigma_y=H(-\mathbf{k})$. Suppose $0<\beta<\kappa_0$, the model (1) has four Weyl nodes at $\pm\mathbf{Q}_\pm$ where $\mathbf{Q}_\pm=(\beta,0,\pm k_0)$ and $k_0=(\kappa_0^2-\beta^2)^{1/2}$.

Near the Weyl nodes, we can linearize the model (1) and rewrite it as a sum of four effective Hamiltonians, each describes the electrons near one of the Weyl nodes: $\mathcal{H}_{\rm w}=\sum_{\gamma=1}^4\sum'_{\mathbf{k}}\Psi^\dagger_{\gamma,\mathbf{k}}H_\gamma(\mathbf{k})\Psi_{\gamma,\mathbf{k}}$, and

$$\begin{aligned} H_{1(2)}(\mathbf{k}) &= (k_x\mp\beta)\sigma_x + k_y\sigma_y + (k_z\mp k_0)\sigma_z,\\ H_{3(4)}(\mathbf{k}) &= (k_x\mp\beta)\sigma_x + k_y\sigma_y + (k_z\pm k_0)\sigma_z, \end{aligned} \quad (2)$$

where k_z has been rescaled by $1/(2k_0)$ and k_y has been rescaled by $1/\alpha$, the indices $\gamma \in \{1,2,3,4\}$ label the Weyl nodes at $\mathbf{Q}_+$, $-\mathbf{Q}_+$, $\mathbf{Q}_-$, and $-\mathbf{Q}_-$, respectively, and $\sum_{\mathbf{k}}'$ indicates that $\mathbf{k}$ is confined to the vicinity of the Weyl nodes. The spinors $\Psi_{\gamma,\mathbf{k}} \equiv (\psi_{\gamma,\uparrow,\mathbf{k}}, \psi_{\gamma,\downarrow,\mathbf{k}})^T$ of the Weyl nodes are given by $\Psi_{1,\mathbf{k}} = \Psi_{3,\mathbf{k}} = [c^{(B)}_{\uparrow,\mathbf{k}}, c^{(A)}_{\downarrow,\mathbf{k}}]^T$ and $\Psi_{2,\mathbf{k}} = \Psi_{4,\mathbf{k}} = [c^{(A)}_{\uparrow,\mathbf{k}}, c^{(B)}_{\downarrow,\mathbf{k}}]^T$ with $c^{(s)}_{\uparrow(\downarrow),\mathbf{k}} = (c_{s,\uparrow,\mathbf{k}} \pm c_{s,\downarrow,\mathbf{k}})/\sqrt{2}$. $H_1(\mathbf{k})$ and $H_2(\mathbf{k})$ describe the two Weyl nodes of positive chirality whereas $H_3(\mathbf{k})$ and $H_4(\mathbf{k})$ describe the two Weyl nodes of negative chirality. All the Weyl nodes consist of different orbitals and spins and exhibit a nontrivial spin/orbital-momentum locking. They form two time-reversed pairs, i.e., $\sigma_y H_1^*(\mathbf{k})\sigma_y = H_2(-\mathbf{k})$ and $\sigma_y H_3^*(\mathbf{k})\sigma_y = H_4(-\mathbf{k})$, each of them with definite chirality.

Next, introducing the s-wave superconducting coupling with both intraorbital and interorbital pairing potentials and projecting onto the spinors of the Weyl nodes, one can see that the interorbital pairing is strongly suppressed due to the mismatch of spins or momenta [65]. Suppose the Weyl nodes are well separated and the chemical potential is close to the Weyl nodes, then only the intraorbital pairing is important and reads $\mathcal{H}_S = \mathcal{H}_S^+ + \mathcal{H}_S^-$ with

$$\mathcal{H}_S^+ = \sum_{\mathbf{k}}{}' [(\Delta_s c^\dagger_{1,\uparrow,\mathbf{k}} c^\dagger_{2,\downarrow,-\mathbf{k}} + \text{H.c.}) + (1 \leftrightarrow 2)], \quad (3)$$

$$\mathcal{H}_S^- = \sum_{\mathbf{k}}{}' [(\Delta_s c^\dagger_{3,\uparrow,\mathbf{k}} c^\dagger_{4,\downarrow,-\mathbf{k}} + \text{H.c.}) + (3 \leftrightarrow 4)]. \quad (4)$$

The pairing potential Δ_s couples electrons on the Weyl nodes stemming from the time-reversed pairs. The whole system can thus be understood as two effectively independent and equivalent subsystems with opposite chirality. In the following, we will discuss the physics of the subsystem with positive chirality.

Using the Nambu spinor in real space for positive chirality $\tilde{\Psi}(\mathbf{r}) = [c_{1,\uparrow}(\mathbf{r}), c_{1,\downarrow}(\mathbf{r}), c_{2,\uparrow}(\mathbf{r}), c_{2,\downarrow}(\mathbf{r}), c^\dagger_{1,\downarrow}(\mathbf{r}), -c^\dagger_{1,\uparrow}(\mathbf{r}), c^\dagger_{2,\downarrow}(\mathbf{r}), -c^\dagger_{2,\uparrow}(\mathbf{r})]^T$, we recast the Hamiltonian in a Bogoliubov–de Gennes (BdG) form: $\mathcal{H}_+ = (1/2)\int d\mathbf{r}\, \Phi^\dagger(\mathbf{r}) H_{\text{BdG}} \Phi(\mathbf{r})$, and

$$H_{\text{BdG}} = (-i\nabla_{\mathbf{r}} \cdot \boldsymbol{\sigma} - \mu\sigma_0)\tau_0\nu_z + |\Delta_s| e^{i\phi\nu_z\sigma_0\tau_x\nu_x}, \quad (5)$$

where $\Delta_s(\mathbf{r}) = |\Delta_s(\mathbf{r})| e^{i\phi(\mathbf{r})}$. We have introduced the identity and Pauli matrices ν_i and τ_i ($i = 0,x,y,z$) for electron-hole and Weyl-node degrees of freedom, respectively, and moved the k_0 and β dependence into the wave function by performing a unitary transformation $\Phi(\mathbf{r}) = e^{i(k_0 z\sigma_z + \beta x\sigma_x)\tau_z\nu_z}\tilde{\Psi}(\mathbf{r})$. In a uniform system, the eigenenergies are given by $\varepsilon = \pm[|\Delta_s|^2 + (|\mathbf{k}| \pm \mu)^2]^{1/2}$. The superconductor is fully gapped. The BdG Hamiltonian (5) decouples into two 4×4 identical blocks which can be treated separately.

Reflection probabilities in a Weyl N-S junction. The time-reversal symmetric Weyl N-S junction can be described by the BdG Hamiltonian (5) with $\Delta_s(z) = \Delta e^{i\phi}\Theta(z)$ and $\mu(z) = \mu_N\Theta(-z) + \mu_S\Theta(z)$. Here, $\Theta(z)$ is the Heaviside step function, $\Delta > 0$, and a constant superconducting phase ϕ are assumed. Experimentally, μ_N and μ_S can be tuned independently by plunger gates. The wave-vector $\mathbf{k}_\parallel = (k_x, k_y)$ parallel to the N-S interface is conserved. We can treat each $\mathbf{k}_\parallel$ separately and work with a quasi-one-dimensional (quasi-1D) junction problem.

Assuming first a clean interface and matching the wave function at the interface, the probabilities of Andreev and normal reflections at an excitation energy $\varepsilon \geqslant 0$, in general, can be expressed as

$$R_{eh}(\varepsilon, \mathbf{k}_\parallel) = |\cos(2\alpha_e)\cos(2\alpha_h)|\,|\sin(\tilde{\alpha}_e - \tilde{\alpha}_h)/\mathcal{Z}|^2, \quad (6)$$

$$R_{ee}(\varepsilon, \mathbf{k}_\parallel) = |\mathcal{Y}/\mathcal{Z}|^2, \quad (7)$$

respectively, where $\mathcal{Z} = e^{i\beta}\cos(\alpha_e + \tilde{\alpha}_e)\sin(\alpha_h + \tilde{\alpha}_h) - e^{-i\beta}\cos(\alpha_e + \tilde{\alpha}_h)\sin(\alpha_h + \tilde{\alpha}_e)$, $\mathcal{Y} = e^{i\beta}\sin(\alpha_e - \tilde{\alpha}_e)\sin(\alpha_h + \tilde{\alpha}_h) - e^{-i\beta}\sin(\alpha_e - \tilde{\alpha}_h)\sin(\alpha_h + \tilde{\alpha}_e)$, $\alpha_{e(h)} = \arctan(k_\parallel/k_{e(h)})/2$, $\tilde{\alpha}_{e(h)} = \arctan(k_\parallel/k_{eq(hq)})/2$, and $k_\parallel = |\mathbf{k}_\parallel|$. The perpendicular momenta for the electron (hole) and electronlike (holelike) quasiparticles are $k_{e(h)} = \text{sgn}(\varepsilon \pm \mu_N + k_\parallel)[(\varepsilon \pm \mu_N)^2 - k_\parallel^2]^{1/2}$ and $k_{eq(hq)} = \text{sgn}\{\varepsilon \pm \text{sgn}(\mu_S \pm k_\parallel)[\Delta^2 + (\mu_S \pm k_\parallel)^2]^{1/2}\}[(\mu_S \pm \Omega)^2 - k_\parallel^2]^{1/2}$, respectively. For subgap energies $\varepsilon \leqslant \Delta$, $\Omega = i(\Delta^2 - \varepsilon^2)^{1/2}$, and $\beta = \arccos(\varepsilon/\Delta)$, whereas for supragap energies $\varepsilon > \Delta$, $\Omega = \text{sgn}(\varepsilon)(\varepsilon^2 - \Delta^2)^{1/2}$, and $\beta = -i\,\text{arccosh}(\varepsilon/\Delta)$. Note that $\alpha_{e(h)}$ is always real whereas $\tilde{\alpha}_{e(h)}$ can be complex. A detailed derivation is provided in the Supplemental Material [65]. For subgap energies, $\varepsilon \leqslant \Delta$, $R_{eh} + R_{ee} = 1$, whereas for supragap energies, $\varepsilon > \Delta$, $R_{eh} + R_{ee} < 1$. For a generic oblique incidence ($\mathbf{k}_\parallel \neq 0$) both normal and Andreev reflections are present, and only for normal incidence ($\mathbf{k}_\parallel = 0$) one has perfect Andreev reflection below the gap since then Eqs. (6) and (7) reduce to $R_{eh} = |e^{-2i\beta}|$ and $R_{ee} = 0$.

Differential conductance. At zero temperature, the differential conductance (per unit area) in the N-S junction is given by [66]

$$\frac{dI}{dV} \equiv \frac{e^2}{h}\int \frac{d^2\mathbf{k}_\parallel}{(2\pi)^2}[1 - R_{ee}(eV, \mathbf{k}_\parallel) + R_{eh}(eV, \mathbf{k}_\parallel)], \quad (8)$$

where eV is the bias voltage. Note that only real k_e's contribute in Eq. (8). We normalize the conductance to the value $G_0 = e^2(\mu_N + eV)^2/(4\pi h)$, corresponding to the number of available channels at energy $\mu_N + eV$ on the N side. With the expressions (6) and (7) in Eq. (8), we are able to analyze the behaviors of the conductance. We concentrate, in the following, on two particular parameter regimes: (i) $\mu_S = \mu_N$ (Δ arbitary); and (ii) $\mu_S \gg \Delta$ (μ_N arbitary) [67], which have a distinct zero-bias feature in common (see below).

For regime (i), $\mu_S = \mu_N$, the normalized conductance $g_{\text{NS}} \equiv G_0^{-1} dI/dV$ [68] as a function of eV is plotted in Fig. 1. At large bias $eV \gg \Delta$, all curves converge to unity. This is expected since at large excitation energies the influence of superconductivity is negligible, which together with an identical chemical potential on both sides makes the interface transparent. The g_{NS}-eV relation is rich in the subgap region, depending on the ratio μ_N/Δ. For $\mu_N/\Delta \gg 1$, the Fermi momentum mismatch of the two sides is negligible, i.e., $k_{eq(hq)} \approx k_{e(h)}$, thus normal reflection is suppressed, leading to perfect Andreev reflection with $g_{\text{NS}} = 2$. Similar behavior occurs for conventional electron systems [66]. For smaller μ_N, but $\mu_N > \Delta$, g_{NS} bends down and even shows a dip at $eV = \Delta$. For $0 < \mu_N < \Delta$, g_{NS} vanishes at $eV = \mu_N$ as no hole state is available for Andreev reflection. This is typical for gapless Dirac systems [69]. In the limit $\mu_N/\Delta \ll 1$, specular Andreev reflection dominates in the bias region $\mu_N < eV < \Delta$ and gives rise

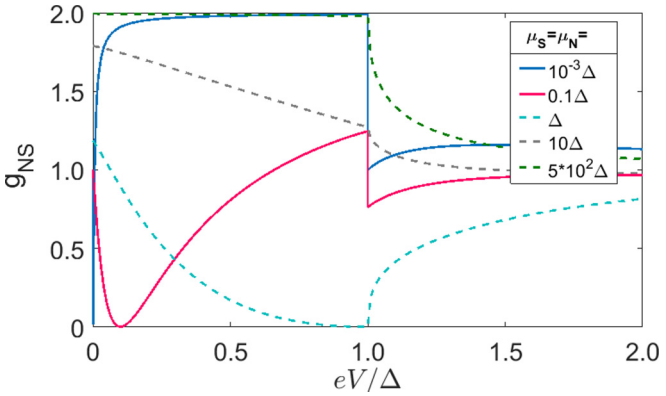

FIG. 1. Normalized conductance g_{NS} as a function of bias for various $\mu_N = \mu_S$'s.

to $g_{NS} = 2$ [65]. Nevertheless, in the limit of low biases, g_{NS} approaches unity for $\mu_N/\Delta \ll 1$ (see the solid curves in Fig. 1), implying the universal conductance e^2/h per channel.

Let us now consider regime (ii), $\mu_S \gg \Delta$, which corresponds to the most relevant experimental condition and is depicted in Fig. 2. For $\mu_N > \mu_S$, g_{NS} varies little in the subgap region, and it decreases smoothly to a constant at large biases. With decreasing μ_N, g_{NS} increases in the subgap region or at large biases. For $\mu_N = \mu_S$, g_{NS} is maximized for any bias and shows perfect Andreev reflection with $g_{NS} = 2$ in the subgap region. For $\mu_N < \Delta$, the vanishing of g_{NS} can also be observed at $eV = \mu_N$ where no Andreev reflection is allowed. Most remarkably, for $\mu_N \ll \mu_S$, one can note again that all the curves approach unity in the limit of low biases, despite that they vary substantially away from zero bias, and converge to a constant $4\ \ln(2) - 2$ at large biases (see the solid curves and inset in Fig. 2).

Zero-bias conductance and universal value. Figure 3 focuses on the behavior of the zero-bias conductance g_{NS}. In particular, Fig. 3(a) displays various salient features of g_{NS} as a function of μ_S and μ_N. First, g_{NS} is centrosymmetric in the phase space $\{\mu_N, \mu_S\}$ as a hallmark of particle-hole symmetry of the system. Second, g_{NS} shows a ridge along the line $\mu_N = \mu_S$ where the small Fermi momentum mismatch strongly

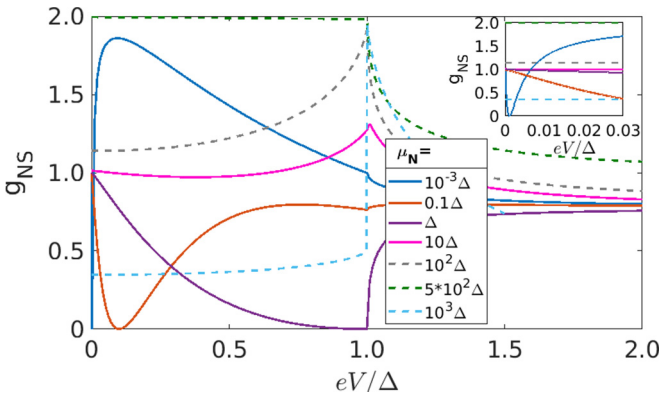

FIG. 2. Normalized conductance g_{NS} as a function of bias for fixed $\mu_S = 5 \times 10^2\Delta$ and various μ_N's. The inset is the zoom-in in the limit of low biases.

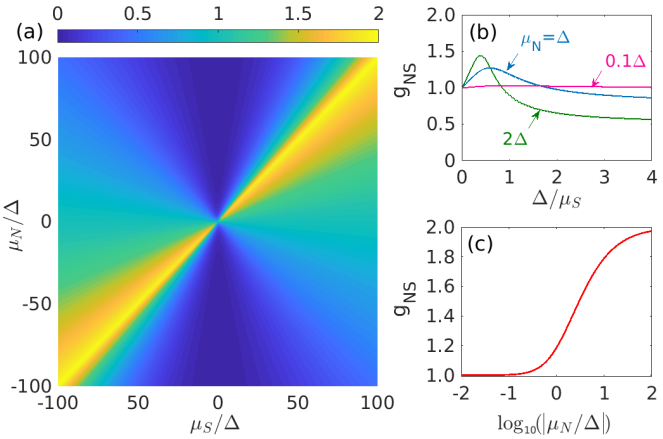

FIG. 3. (a) The zero-bias conductance g_{NS} as a function of μ_S and μ_N. (b) g_{NS} as a function of Δ/μ_S for various μ_N's. (c) Semilogarithmic plot of g_{NS} as a function of $\mu_S = \mu_N$.

suppresses normal reflection. In contrast, when $|\mu_S| \ll |\mu_N|$, the Fermi momentum mismatch is large and normal reflection is enhanced, we have thus vanishing g_{NS}. Finally, g_{NS} is always smaller than unity in the bipolar regime with $\mu_N\mu_S < 0$, implying that the normal reflection contribution is larger than the Andreev reflection contribution.

Figure 3(b) shows the behavior of g_{NS} as a function of Δ/μ_S for various values of μ_N. Figure 3(c) instead displays g_{NS} with respect to $\mu_N = \mu_S$. The universal conductance e^2/h clearly appears in the regime,

$$|\mu_N| \ll \sqrt{\Delta^2 + \mu_S^2}, \tag{9}$$

where the Fermi momenta on the two sides of the interface are very different, i.e, $|k_e| \ll |k_{eq}|$. Such a regime corresponds to an ideal semimetal phase on the N side. To understand the occurrence of the universal conductance, we focus on the regime (9) and analyze our analytical results. Since only real k_e's contribute to the conductance given by Eq. (8), the channels with $k_\parallel < |\mu_N|$ are relevant. From the BdG Hamiltonian (5), we observe that, although on the N side the parallel wave-vector $\mathbf{k}_\parallel$, which couples different spins and orbitals, is significant, on the S side it becomes negligible compared to the perpendicular momentum, i.e., $k_\parallel \ll |k_{eq}| \approx (\Delta^2 + \mu_S^2)^{1/2}$. Thus, the A- and B-orbital components are decoupled from each other on the S side. As a result, the reflection probabilities at zero energy reduce to

$$R_{eh}(0,\mathbf{k}_\parallel) = 1 - |k_\parallel/\mu_N|^2, \tag{10}$$

$$R_{ee}(0,\mathbf{k}_\parallel) = |k_\parallel/\mu_N|^2. \tag{11}$$

They become functions of a single parameter $|k_\parallel/\mu_N|$. Notably, normal and Andreev reflections have opposite contributions to the conductance, according to Eq. (8). Plugging Eqs. (10) and (11) into Eq. (8), it is straightforward to see that the contributions from Andreev and normal reflections cancel each other perfectly, giving rise to the universal conductance e^2/h per channel. The perfect cancellation in the 3D Weyl junction can be understood as a result of the unique spin/orbital-momentum locking and s-wave pairing, which can be inferred from the

analog of the Weyl system to a 1D ferromagnet-superconductor junction [65].

Robustness of the universal value. We note that in a conventional electron system with a parabolic spectrum, the zero-bias conductance can also exhibit a universal value in the regime (9). However, it is trivially zero. Indeed, since in that case velocity and current are linear in momentum, for large momentum mismatch, the conservation of flux at the interface is only possible if the flux vanishes. By contrast, in a Dirac system, the Fermi velocity is constant, and the flux conservation is less sensitive to the Fermi momentum mismatch. As a consequence, nonvanishing flux and conductance are possible. In graphene, a two-dimensional (2D) Dirac system, a finite characteristic value ($4e^2/3h$) of the zero-bias conductance has been predicted [69]. However, the instabilities of the 2D Dirac cone to small perturbations, such as the intrinsic spin-orbit coupling [70] or the coupling to the substrate [71], likely mask such an effect. In fact, to the authors' knowledge, the value of $4e^2/3h$ in graphene has never been observed experimentally. By contrast, the Weyl nodes in a WSM are topologically protected and cannot be gapped out. We assume uncoupled Weyl nodes which should be valid in clean systems close to charge neutrality. Weak disorder and small deviations from charge neutrality are tolerable as the corrections to the conductance are small compared to e^2/h per channel.

The universal conductance predicted by us is robust even in the presence of an interface barrier due to Klein tunneling [65,72]. The interface barrier can be modeled by a potential term $V_0\Theta(z+d)\Theta(-z)v_z$ in the BdG Hamiltonian where the barrier length $d \to 0$ and potential $V_0 \to \infty$ but the barrier strength $\chi \equiv V_0 d$ remains finite [73]. Then, $g_{\rm NS}$ is an oscillation function of χ with a period π. In the regime (9), $g_{\rm NS}$ oscillates slightly around the universal value as shown in Fig. 4. Note that, if the system is not deep in the regime (9), only a small deviation from e^2/h appears. Therefore, the universal conductance can be used as a distinct signature for time-reversal symmetric Weyl fermions.

Experimental relevance. Recently, an ideal time-reversal symmetric WSM phase has been proposed in HgTe and LaPtBi under compressive strain [38,39]. Additionally, $CuTlSe_2$, $AgTlTe_2$, $AuTlTe_2$, and $ZnPbAs_2$ have been identified as further promising materials with similar properties [40]. There are likely four pairs of Weyl nodes in these systems [39,40]. However, as long as the Fermi energy is close enough to the Weyl nodes and the system is clean, the system can be decoupled into multiple equivalent time-reversed subsystems.

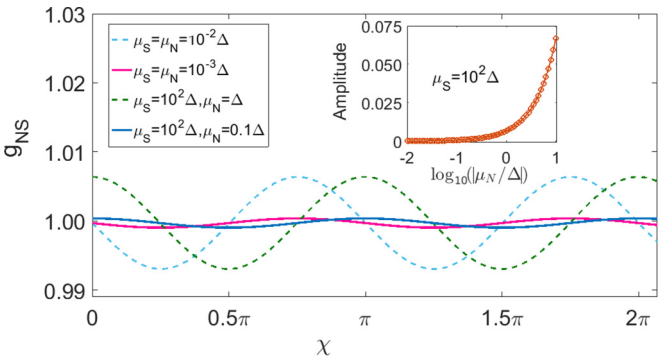

FIG. 4. The zero-bias conductance $g_{\rm NS}$ as a function of the barrier strength χ for various μ_S's and μ_N's. The inset is the semilogarithmic plot of the oscillation amplitudes as a function of μ_N for fixed $\mu_S = 10^2\Delta$.

Then our analysis and main results should hold. Take HgTe, for instance, the energy regime for the Weyl semimetal phase is roughly (−0.25,0.25 meV), extracted from Ref. [39], which should be experimentally detectable. Importantly, superconductivity in compressively strained HgTe could be realized by proximity to a conventional s-wave superconductor, similar to the case of tensilely strained HgTe, a 3D topological insulator [74,75]. Therefore, we expect that the universal conductance e^2/h could be measured in these time-reversal symmetric WSM systems.

Finally, we note that, in time-reversal-broken Weyl semimetals, the chirality blockade may completely suppress Andreev reflection and hence the conductance [62]. Thus, the results found here are not applicable to these time-reversal-broken systems.

Summary. We have analyzed a time-reversal symmetric Weyl N-S junction with an s-wave superconducting state. In an accessible regime, the zero-bias differential conductance takes the universal value of e^2/h per channel, independent of the pairing and chemical potentials as the Andreev and normal reflection contributions perfectly cancel at vanishing excitation energy. The universal conductance can be understood as a consequence of the interplay of the unique spin/orbital-momentum locking and s-wave pairing in the WSM system.

Acknowledgments. We thank J. Li, B. Scharf, M. Stehno, and X. Wu for valuable discussions. This work was supported by by the DFG (Grants No. SPP1666 and No. SFB1170 "ToCoTronics") and the ENB Graduate School on "Topological Insulators."

[1] X. Wan, A. M. Turner, A. Vishwanath, and S. Y. Savrasov, Phys. Rev. B **83**, 205101 (2011).
[2] A. M. Turner and A. Vishwanath, arXiv:1301.0330.
[3] P. Hosur and X. Qi, C. R. Phys. **14**, 857 (2013).
[4] N. P. Armitage, E. J. Mele, and A. Vishwanath, arXiv:1705.01111.
[5] H. B. Nielsen and M. Ninomiya, Phys. Lett. **105B**, 219 (1981).
[6] H. B. Nielsen and M. Ninomiya, Phys. Lett. **130B**, 389 (1983).
[7] V. Aji, Phys. Rev. B **85**, 241101 (2012).
[8] P. Goswami and S. Tewari, Phys. Rev. B **88**, 245107 (2013).
[9] C.-X. Liu, P. Ye, and X.-L. Qi, Phys. Rev. B **87**, 235306 (2013).
[10] K. Fukushima, D. E. Kharzeev, and H. J. Warringa, Phys. Rev. D **78**, 074033 (2008).
[11] G. Xu, H. M. Weng, Z. J. Wang, X. Dai, and Z. Fang, Phys. Rev. Lett. **107**, 186806 (2011).
[12] K. Y. Yang, Y. M. Lu, and Y. Ran, Phys. Rev. B **84**, 075129 (2011).
[13] A. A. Zyuzin and A. A. Burkov, Phys. Rev. B **86**, 115133 (2012).
[14] P. Hosur, S. A. Parameswaran, and A. Vishwanath, Phys. Rev. Lett. **108**, 046602 (2012).
[15] D. T. Son and B. Z. Spivak, Phys. Rev. B **88**, 104412 (2013).
[16] A. A. Burkov, Phys. Rev. Lett. **113**, 187202 (2014).

[17] E. V. Gorbar, V. A. Miransky, and I. A. Shovkovy, Phys. Rev. B **89**, 085126 (2014).
[18] A. A. Burkov, Phys. Rev. Lett. **113**, 247203 (2014).
[19] A. C. Potter, I. Kimchi, and A. Vishwanath, Nat. Commun. **5**, 5161 (2014).
[20] H.-Z. Lu, S.-B. Zhang, and S.-Q. Shen, Phys. Rev. B **92**, 045203 (2015).
[21] S. A. Parameswaran, T. Grover, D. A. Abanin, D. A. Pesin, and A. Vishwanath, Phys. Rev. X **4**, 031035 (2014).
[22] J. Zhou, H. R. Chang, and D. Xiao, Phys. Rev. B **91**, 035114 (2015).
[23] S.-B. Zhang, H.-Z. Lu, and S.-Q. Shen, New J. Phys. **18**, 053039 (2016).
[24] C. Zhang, S. Y. Xu, I. Belopolski, Z. Yuan, Z. Lin, B. Tong, N. Alidoust, C. C. Lee, S. M. Huang, T. R. Chang, H. T. Jeng, H. Lin, M. Neupane, D. S. Sanchez, H. Zheng, G. Bian, J. Wang, C. Zhang, H. Z. Lu, S. Q. Shen, T. Neupert, M. Z. Hasan, and S. Jia, Nat. Commun. **7**, 10735 (2016).
[25] Q. Li, D. E. Kharzeev, C. Zhang, Y. Huang, I. Pletikosic, A. V. Fedorov, R. D. Zhong, J. A. Schneeloch, G. D. Gu, and T. Valla, Nat. Phys. **12**, 550 (2016).
[26] A. A. Burkov and L. Balents, Phys. Rev. Lett. **107**, 127205 (2011).
[27] G. B. Halász and L. Balents, Phys. Rev. B **85**, 035103 (2012).
[28] M. Hirayama, R. Okugawa, S. Ishibashi, S. Murakami, and T. Miyake, Phys. Rev. Lett. **114**, 206401 (2015).
[29] J. Liu and D. Vanderbilt, Phys. Rev. B **90**, 155316 (2014).
[30] S. Y. Xu, I. Belopolski, N. Alidoust, M. Neupane, G. Bian, C. L. Zhang, R. Sankar, G. Q. Chang, Z. J. Yuan, C. C. Lee, S. M. Huang, H. Zheng, J. Ma, D. S. Sanchez, B. K. Wang, A. Bansil, F. C. Chou, P. P. Shibayev, H. Lin, S. Jia, and M. Z. Hasan, Science **349**, 613 (2015).
[31] L. X. Yang, Z. K. Liu, Y. Sun, H. Peng, H. F. Yang, T. Zhang, B. Zhou, Y. Zhang, Y. F. Guo, M. Rahn, D. Prabhakaran, Z. Hussain, S.-K. Mo, C. Felser, B. Yan, and Y. L. Chen, Nat. Phys. **11**, 728 (2015).
[32] B. Q. Lv, H. M. Weng, B. B. Fu, X. P. Wang, H. Miao, J. Ma, P. Richard, X. C. Huang, L. X. Zhao, G. F. Chen, Z. Fang, X. Dai, T. Qian, and H. Ding, Phys. Rev. X **5**, 031013 (2015).
[33] B. Q. Lv, N. Xu, H. M. Weng, J. Z. Ma, P. Richard, X. C. Huang, L. X. Zhao, G. F. Chen, C. E. Matt, F. Bisti, V. N. Strocov, J. Mesot, Z. Fang, X. Dai, T. Qian, M. Shi, and H. Ding, Nat. Phys. **11**, 724 (2015).
[34] S. Y. Xu, N. Alidoust, I. Belopolski, Z. Yuan, G. Bian, T. R. Chang, H. Zheng, V. N. Strocov, D. S. Sanchez, G. Chang, C. Zhang, D. Mou, Y. Wu, L. Huang, C. C. Lee, S. M. Huang, B. Wang, A. Bansil, H. T. Jeng, T. Neupert, A. Kaminski, H. Lin, S. Jia, and M. Zahid Hasan, Nat. Phys. **11**, 748 (2015).
[35] N. Xu, H. M. Weng, B. Q. Lv, C. E. Matt, J. Park, F. Bisti, V. N. Strocov, D. Gawryluk, E. Pomjakushina, K. Conder, N. C. Plumb, M. Radovic, G. Autes, O. V. Yazyev, Z. Fang, X. Dai, T. Qian, J. Mesot, H. Ding, and M. Shi, Nat. Commun. **7**, 11006 (2016).
[36] S. M. Huang, S. Y. Xu, I. Belopolski, C. C. Lee, G. Chang, B. K. Wang, N. Alidoust, G. Bian, M. Neupane, C. Zhang, S. Jia, A. Bansil, H. Lin, and M. Z. Hasan, Nat. Commun. **6**, 7373 (2015).
[37] H. M. Weng, C. Fang, Z. Fang, B. A. Bernevig, and X. Dai, Phys. Rev. X **5**, 011029 (2015).
[38] T. Rauch, S. Achilles, J. Henk, and I. Mertig, Phys. Rev. Lett. **114**, 236805 (2015).
[39] J. Ruan, S.-K. Jian, H. Yao, H. Zhang, S.-C. Zhang, and D. Xing, Nat. Commun. **7**, 11136 (2016).
[40] J. Ruan, S.-K. Jian, D. Zhang, H. Yao, H. Zhang, S.-C. Zhang, and D. Xing, Phys. Rev. Lett. **116**, 226801 (2016).
[41] S. Jia, S.-Y. Xu, and M. Z. Hasan, Nature Mater. **15**, 1140 (2016).
[42] S. Murakami, M. Hirayama, R. Okugawa, and T. Miyake, Sci. Adv. **3**, e1602680 (2017).
[43] T. Meng and L. Balents, Phys. Rev. B **86**, 054504 (2012).
[44] G. Y. Cho, J. H. Bardarson, Y.-M. Lu, and J. E. Moore, Phys. Rev. B **86**, 214514 (2012).
[45] S. A. Yang, H. Pan, and F. Zhang, Phys. Rev. Lett. **113**, 046401 (2014).
[46] P. Hosur, X. Dai, Z. Fang, and X.-L. Qi, Phys. Rev. B **90**, 045130 (2014).
[47] U. Khanna, A. Kundu, S. Pradhan, and S. Rao, Phys. Rev. B **90**, 195430 (2014).
[48] H. Wei, S.-P. Chao, and V. Aji, Phys. Rev. B **89**, 014506 (2014).
[49] G. Bednik, A. A. Zyuzin, and A. A. Burkov, Phys. Rev. B **92**, 035153 (2015).
[50] B. Lu, K. Yada, M. Sato, and Y. Tanaka, Phys. Rev. Lett. **114**, 096804 (2015).
[51] Y. Li and F. D. M. Haldane, arXiv:1510.01730.
[52] S.-K. Jian, Y.-F. Jiang, and H. Yao, Phys. Rev. Lett. **114**, 237001 (2015).
[53] B. Liu, X. Li, L. Yin, and W. V. Liu, Phys. Rev. Lett. **114**, 045302 (2015).
[54] A. Chen and M. Franz, Phys. Rev. B **93**, 201105 (2016).
[55] R. Wang, L. Hao, B. Wang, and C. S. Ting, Phys. Rev. B **93**, 184511 (2016).
[56] M. D. Bachmann, N. Nair, F. Flicker, R. Ilan, T. Meng, N. J. Ghimire, E. D. Bauer, F. Ronning, J. G. Analytis, and P. J. W. Moll, Sci. Adv. **3**, e1602983 (2017).
[57] S. Uchida, T. Habe, and Y. Asano, J. Phys. Soc. Jpn. **83**, 064711 (2014).
[58] W. Chen, L. Jiang, R. Shen, L. Sheng, B. G. Wang, and D. Y. Xing, Europhys. Lett. **103**, 27006 (2013).
[59] Y. Kim, M. J. Park, and M. J. Gilbert, Phys. Rev. B **93**, 214511 (2016).
[60] U. Khanna, D. K. Mukherjee, A. Kundu, and S. Rao, Phys. Rev. B **93**, 121409 (2016).
[61] K. A. Madsen, E. J. Bergholtz, and P. W. Brouwer, Phys. Rev. B **95**, 064511 (2017).
[62] N. Bovenzi, M. Breitkreiz, P. Baireuther, T. E. O'Brien, J. Tworzydło, I. Adagideli, and C. W. J. Beenakker, Phys. Rev. B **96**, 035437 (2017).
[63] D. K. Mukherjee, S. Rao, and A. Kundu, Phys. Rev. B **96**, 161408 (2017).
[64] This model is based on the lattice model proposed by S. Kourtis, J. Li, Z. Wang, A. Yazdani, and B. A. Bernevig, Phys. Rev. B **93**, 041109 (2016).
[65] See Supplemental Material at http://link.aps.org/supplemental/10.1103/PhysRevB.97.041116 for detailed calculations and analysis.
[66] G. E. Blonder, M. Tinkham, and T. M. Klapwijk, Phys. Rev. B **25**, 4515 (1982).
[67] But μ_N and μ_S are still small enough so that the linearized model (2) is applicable.
[68] Here and everywhere afterwards we refer the normalized conductance to $g_{\rm NS}$.
[69] C. W. J. Beenakker, Phys. Rev. Lett. **97**, 067007 (2006).

[70] C. L. Kane and E. J. Mele, Phys. Rev. Lett. **95**, 226801 (2005).
[71] G. Giovannetti, P. A. Khomyakov, G. Brocks, P. J. Kelly, and J. van den Brink, Phys. Rev. B **76**, 073103 (2007).
[72] M. I. Katsnelson, K. S. Novoselov, and A. K. Geim, Nat. Phys. **2**, 620 (2006).
[73] S. Bhattacharjee and K. Sengupta, Phys. Rev. Lett. **97**, 217001 (2006).
[74] L. Maier, J. B. Oostinga, D. Knott, C. Brüne, P. Virtanen, G. Tkachov, E. M. Hankiewicz, C. Gould, H. Buhmann, and L. W. Molenkamp, Phys. Rev. Lett. **109**, 186806 (2012).
[75] J. Wiedenmann, E. Liebhaber, J. Kübert, E. Bocquillon, P. Burset, C. Ames, H. Buhmann, T. M. Klapwijk, and L. W. Molenkamp, Phys. Rev. B **96**, 165302 (2017).